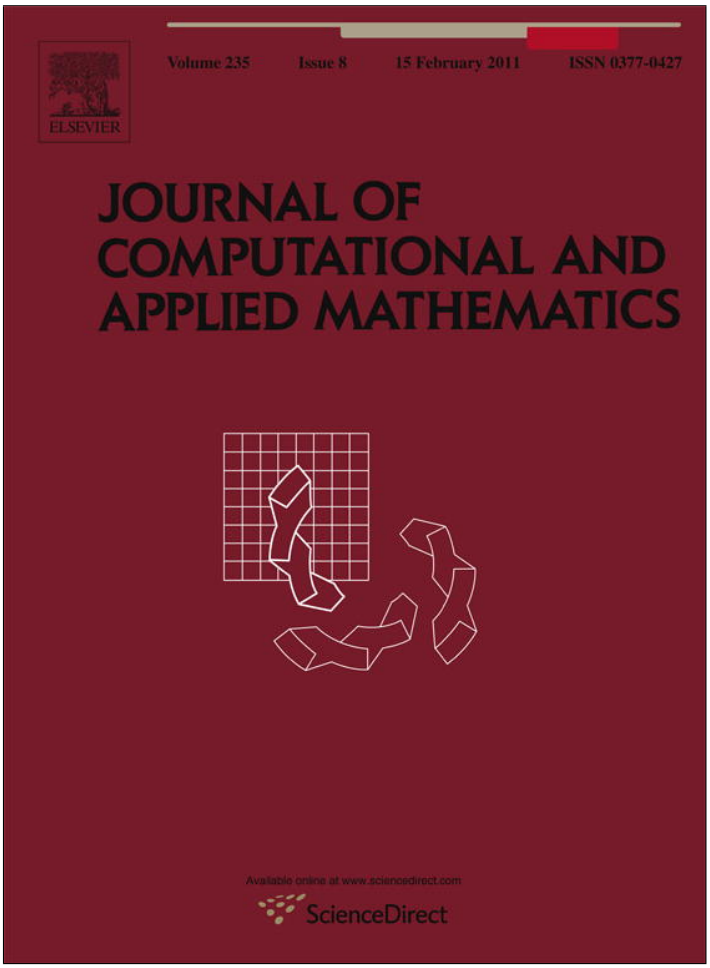

Journal of Computational and Applied Mathematics 235 (2011) 2030–2040

Contents lists available at ScienceDirect

Journal of Computational and Applied Mathematics

journal homepage: www.elsevier.com/locate/cam

# An exact Riemann solver and a Godunov scheme for simulating highly transient mixed flows

F. Kerger*, P. Archambeau, S. Erpicum, B.J. Dewals, M. Pirotton

*Research Unit of Hydrology, Applied Hydrodynamics and Hydraulic Constructions (HACH), Department ArGEnCo, University of Liege, 1, allée des chevreuils, 4000-Liège-Belgium, Belgium*

ARTICLE INFO

*Article history:*
Received 26 August 2009
Received in revised form 24 August 2010

*Keywords:*
Hydraulics
Finite volume method
Negative Preissmann slot
Saint-Venant equations
Transient flow
Water hammer

ABSTRACT

The current research *aims* at deriving a one-dimensional numerical model for describing highly transient mixed flows. In particular, this paper focuses on the development and assessment of a unified numerical scheme adapted to describe free-surface flow, pressurized flow and mixed flow (characterized by the simultaneous occurrence of free-surface and pressurized flows). The *methodology* includes three steps. First, the authors derived a unified mathematical model based on the Preissmann slot model. Second, a first-order explicit finite volume Godunov-type scheme is used to solve the set of equations. Third, the numerical model is assessed by comparison with analytical, experimental and numerical results. The key *results* of the paper are the development of an original negative Preissmann slot for simulating sub-atmospheric pressurized flow and the derivation of an exact Riemann solver for the Saint-Venant equations coupled with the Preissmann slot.



## 1. Introduction

Mixed flows, characterized by the simultaneous occurrence of free-surface and pressurized flows, are frequently encountered in river networks, sewer systems, storm-water storage pipes, flushing galleries in dams, …. As a matter of fact, some hydraulic structures are designed to combine free-surface sections and pressurized sections (e.g. water intake). In addition, dynamic pipe filling bores may occur in hydraulic structures designed only for conveying free-surface flow under an extreme water inflow or upon starting a pump. During such a transition, highly transient phenomena appear and may cause structural damage to the systems [1,2], generate geysers through vertical shafts [3], induce flooding, …. What is more, air/water interactions may arise, particularly at the transition bore [4]. A good prediction of pressure generated is therefore an industrial necessity. Still, numerical simulation of mixed flow remains challenging for two main reasons. First, the dissimilarity between the sets of equations describing free-surface and pressurized flows has to be overcome. Second, air/water interaction should be taken into account by means of a two-phase flow model.

Different mathematical approaches to the description of mixed flows have been developed to date. First, the so-called *shock-tracking approach* consists of obtaining separately free-surface and pressurized flows through different sets of equations [5–7]. Transitions between the free-surface and the pressurized flow are tracked explicitly and regarded as internal boundaries across which appropriate jump conditions are imposed. The advantage of the approach is that the transition is computed as a true discontinuity (infinite resolution). However, the associated algorithms are very complex and become far too complicated or simply impossible to apply for complex wave interaction and multi-dimensional problems, which is the major drawback of the approach. Second, the rigid water column approach [8] treats each phase (air/water) separately on the basis of a specific set of equations. The approach manages to simulate complex configurations of the

* Corresponding author. Tel.: +32 43 66 90 04.
*E-mail address:* fkerger@ulg.ac.be (F. Kerger).

0377-0427/$ – see front matter © 2010 Elsevier B.V. All rights reserved.
doi:10.1016/j.cam.2010.09.026

transition. However, the complexity of the method prevents its use for practical application. Third, the so-called "shock-capturing" approach (by analogy with shock-capturing numerical schemes) computes pressurized and free-surface flows by using a single set of equations. The main advantage of the method is that there is no need to track the interface explicitly. To our knowledge, four mathematical models fall into this category: the *Preissmann slot* method [9], the *two-component pressure* approach [10], the dual model [11] and the kinetic model [12]. It can be shown that the three former sets of equations are analogous except in the way that they interpret the conserved variables. As a consequence, their mathematical properties are similar.

In this paper, the Preissmann slot model has been used mainly because of its simplicity. Free-surface flow and pressurized flow are equally obtained through the free-surface set of equations by just adding a narrow slot at the top of the pipe. However, the method exposes two major shortcomings [7]. First, the mathematical model prohibits the formation of sub-atmospheric pressures. Second, spurious numerical post-transition oscillations appear because of the steep change in the wave celerity (from $\sim$10 m/s up to $\sim$1000 m/s) across the transition. The origin of these oscillations has been investigated in [13].

The current research aims at deriving a one-dimensional numerical model for describing highly transient mixed flows, and consequently at finding adequate solutions to these two shortcomings. From a mathematical point of view, the Preissmann slot concept is in the following not only used but extended in an original form, that we named the *negative Preissmann slot*, to simulate sub-atmospheric pressurized flows while keeping the equations in the Preissmann format. It is shown to provide a consistent answer to the first shortcoming of the Preissmann slot model. From a numerical point of view, several schemes have been developed for solving the Saint-Venant equations in conjunction with a Preissmann slot. Let us especially mention the implicit TVD finite volume scheme developed in [14], the MUSCL–Hancock method used in [15] or the Roe-like scheme with a special treatment for the transition introduced in [11]. All of these are unsuccessful in eliminating spurious oscillations. That is why we propose herein a new robust finite volume scheme which reduces spurious post-transition oscillations. It is based on the Godunov method in conjunction with a new exact Riemann solver for mixed flows in rectangular and circular pipes. Assessment of the model is performed by comparison with analytical and experimental results.

## 2. The mathematical model

One-dimensional unsteady open channel flow is described by a set of hyperbolic partial differential equations (PDE's) usually called Saint-Venant equations [16]. The Saint-Venant equations are derived from area-integrating the Navier–Stokes equations under the following series of assumptions: the flow is one-dimensional with a uniform velocity in the cross-section; the streamline curvature is small and vertical accelerations are negligible, and hence the pressure is hydrostatic; there is no lateral inflow; and the effects of boundary friction and turbulence can be accounted for through resistance laws analogous to those used for steady state flow. This results in the following PDE's:

$$\frac{\partial}{\partial t}\begin{pmatrix} A \\ Q \end{pmatrix} + \frac{\partial}{\partial x}\begin{pmatrix} Q \\ Q^2/A + gI_1 \end{pmatrix} = \begin{pmatrix} 0 \\ gA\left(S_0 - S_f\right) + gI_2 \end{pmatrix} \tag{1}$$

$$\text{with } I_1(h) = \int_{-h_b}^{h_{fs}} (h-\xi)\, l(x,\xi)\, \mathrm{d}\xi \quad \text{and} \quad I_2(h) = \int_{-h_b}^{h_{fs}} (h-\xi)\, \frac{\partial l(x,\xi)}{\partial x}\mathrm{d}\xi \tag{2}$$

where $A[\mathrm{m}^2]$ is the flow area, $Q[\mathrm{m}^3/\mathrm{s}]$ is the flow discharge, $g[\mathrm{m}^2/\mathrm{s}]$ is the gravity, $S_0$ [–] is the bed slope, $S_f$ [–] is the friction term resulting from the resistance law, $h$ [m] is the water height, $l$ [m] is the free-surface width, $h_{fs}$ [m] is the free-surface elevation and $h_b$ [m] is the bottom elevation. The friction term $S_f$ is assumed to be given by the Manning–Strickler relation:

$$S_f = \frac{Q\,|Q|}{A^2K^2R_h^{4/3}} \tag{3}$$

where $K$ is the Strickler coefficient and $R_h$ [m] the hydraulic radius.

Pressurized flows are commonly described through the Allievi equations [17]. According to the Preissmann slot model [9], pressurized flow can equally be calculated through the Saint-Venant equations by adding a conceptual slot on the top of a closed pipe (Fig. 1(b)). When the water level is above the pipe crown, it provides a conceptual free-surface flow, whose gravity wavespeed is $c = \sqrt{g\Omega/T_s}$ ($T_s$ is the slot width). Strictly speaking, the water hammer wavespeed, referred to as $a[\mathrm{m/s}]$, depends on the properties of the fluid, the pipe, and its means of support. In a first approximation, its value is not dependent on the pressure value and may be computed on the basis of solid mechanics relations [17]. It is then easy to choose a slot width $T_s$ which equalizes the gravity wavespeed $c$ to the water hammer wavespeed $a$:

$$T_s \triangleq \frac{g\Omega}{a^2} \quad \text{with } a^2 \triangleq A\frac{\mathrm{d}p}{\mathrm{d}(\rho A)} = \frac{g\Delta h}{\Delta A/A + \Delta\rho/\rho}. \tag{4}$$

Physically, the slot accounts naturally for the water compressibility and the pipe dilatation under a variation of pressure.

Since all the relevant hydraulic information is summarized in the relation water height/flow area ($H/A$), geometry of the pipe is simply provided by such a function. A specific relation corresponds to each geometry of the cross-section

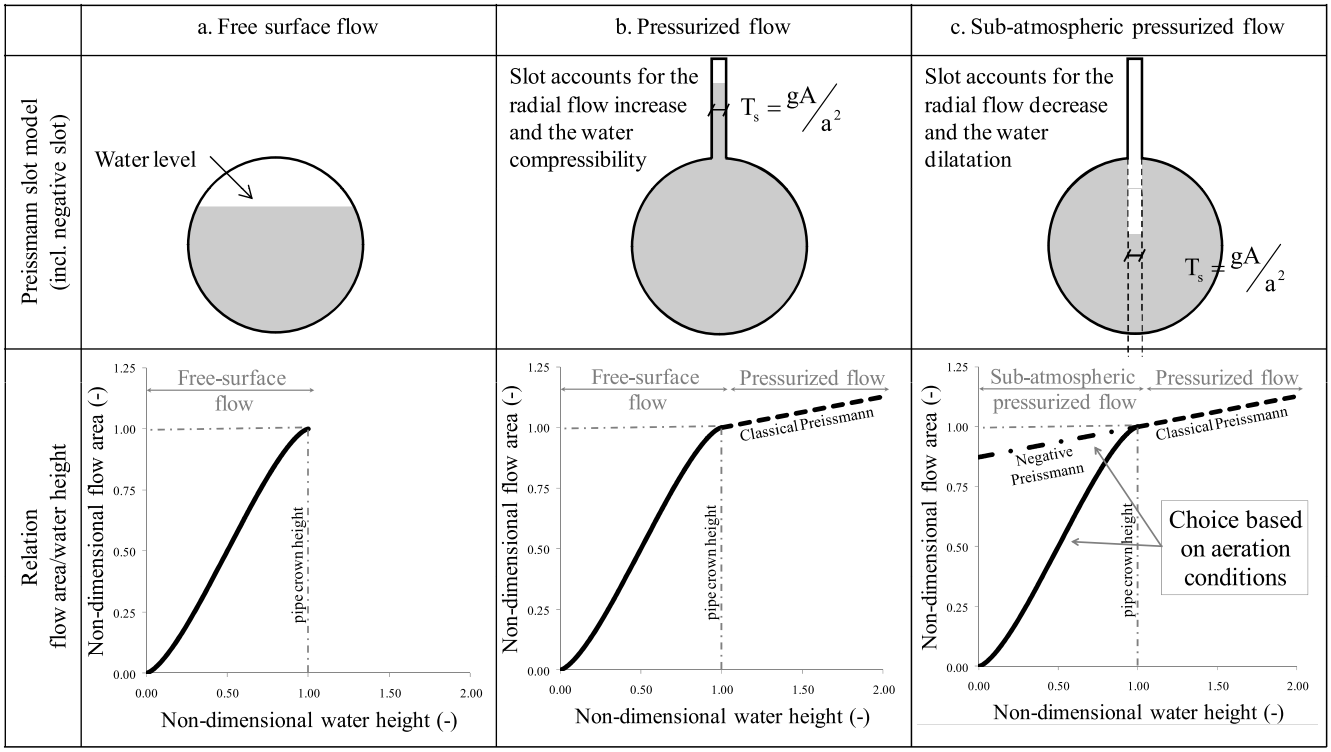


**Fig. 1.** The Preissmann slot method under different flow conditions.

(Fig. 1(a)). Adding the Preissmann slot leads to linear extension of the relation beyond the pipe crown head. In order to simulate pressurized flows with a piezometric head below the pipe crown, the authors propose a new concept, called the *negative Preissmann slot*. It consists of extending the Preissmann straight line for the water height below the pipe crown (Fig. 1(c)). To each water height below the pipe crown there correspond two values of the flow area: one for the free-surface flow and one for the pressurized flow. It is chosen between the two relations according to the local aeration conditions.

## 3. The finite volume numerical scheme

Godunov-type methods have proven popular for treating non-linear systems of partial differential equations due to their ability to treat discontinuities arising in the solution [18,19]. The Godunov method consists in considering conservative variables as piecewise constant over the mesh cells at each time step. The time evolution is determined by the solution of the Riemann problem arising at each mesh boundary.

Let's consider the homogeneous part of Eq. (1):

$$\frac{\partial}{\partial t}\mathbf{U} + \frac{\partial}{\partial x}F(\mathbf{U}) = 0 \tag{5}$$

where the vectors of the conserved variable and flux are

$$\mathbf{U} = \begin{pmatrix} A \\ Q \end{pmatrix} \quad \text{and} \quad \mathbf{F} = \begin{pmatrix} Q \\ Q^2/A + gI_1 \end{pmatrix}. \tag{6}$$

Integration of (5) over finite volumes leads to the updating conservative formula [18,19]:

$$\mathbf{U}_i^{n+1} = \mathbf{U}_i^n - \frac{\Delta t}{\Delta x}\left[F_{i+1/2} - F_{i-1/2}\right] \tag{7}$$

where $F_{i+1/2}$ is the intercell numerical flux corresponding to the intercell boundary at $x = x_{i+1/2}$ between $i$ and $i+1$. The Godunov flux $F_{i+1/2}$ is defined [18] as the physical flux function $\mathbf{F}(\mathbf{U})$ evaluated at the solution $\mathbf{U}_{i+1/2}(x/t = 0)$ of the Riemann problem at the intercell boundary. Two items are needed to evaluate the Godunov flux. First, we need the solution $\mathbf{U}_{i+1/2}(x/t)$ of the Riemann problem with data $\mathbf{U}_L = \mathbf{U}_i^n$ (left) and $\mathbf{U}_R = \mathbf{U}_{i+1}^n$ (right). Second, we need a sampling procedure in order to identify the solution along the $t$-axis $x/t = 0$.

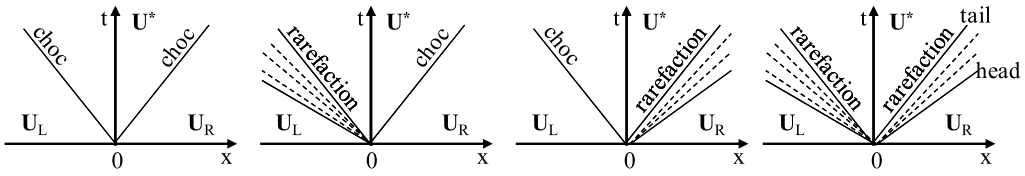


**Fig. 2.** Wave configuration in the solution of the Riemann problem.

### 3.1. The Riemann problem

The Riemann problem for the homogeneous Saint-Venant equations (5) is defined as the initial-value problem (IVP) with piecewise constant initial data (where the subscripts $L$ and $R$ denote left and right states respectively):

$$\begin{aligned} &\frac{\partial}{\partial t}\mathbf{U}+\frac{\partial}{\partial x}\mathbf{F}(\mathbf{U})=0\\ &\mathbf{U}(x,0)=\begin{cases}\mathbf{U}_L & \text{if } x<0\\ \mathbf{U}_R & \text{if } x>0.\end{cases}\end{aligned} \tag{8}$$

The IVP can be solved exactly and the solution can be represented in the $xt$-plane (Fig. 2). Two waves, one travelling to the left and the other to the right, can be either shock or rarefaction waves. The waves separate three states, namely $U_L$, $U_R$ and $U^*$ (the star region). Toro [18] proposes an efficient exact Riemann solver for the shallow water equation. For the Saint-Venant equation, various approximate Riemann solvers have been developed. Let us mention the linearized Roe-like solvers of Glaister [20] and of Bourdarias [11], and the two-shocks approximation of Leon [15].

The authors propose here an efficient Riemann exact solver for solving the Saint-Venant equations by analogy with the work of Toro [18] on shallow water equations. We derive a single non-linear algebraic equation for the flow area $A^*$ in the star region, namely

$$f\left(A^*\right)\equiv f_L\left(A^*,A_L\right)+f_R\left(A^*,A_R\right)+u_R-u_L=0 \tag{9}$$

where $u_L$ and $u_R$ are velocities of the left and right states respectively and $f_L$ and $f_R$ are functions governing conserved quantities across the left and right waves respectively. We make use of either generalized Riemann invariants or Rankine–Hugoniot conditions according to the nature of the wave (rarefaction or shock wave).

### 3.2. Shock waves

As introduced in [18], we suppose that the left wave is a shock travelling with velocity $S_L$ and we consider a steady frame of reference moving with the shock speed. The conservation laws (5) and (6) give

$$\begin{cases}\hat{u}^*=u^*-S_L\\ \hat{u}_L=u_L-S_L\end{cases}\Rightarrow\begin{cases}A^*\hat{u}^*=A_L\hat{u}_L\triangleq M_L\\ A^*\hat{u}^{*2}+gI_1\left(A^*\right)=A_L\hat{u}_L^2+gI_1\left(A_L\right).\end{cases} \tag{10}$$

Inserting $M_L$ in the momentum equation gives

$$M_L\left(\hat{u}^*-\hat{u}_L\right)=gI_1\left(A_L\right)-gI_1\left(A^*\right). \tag{11}$$

From the continuity equation (10), we have $\hat{u}^*=M_L/A^*$ and $\hat{u}_L=M_L/A_L$. After some algebraic manipulations, (11) becomes

$$M_L=\sqrt{\frac{\left[gI_1\left(A_L\right)-gI_1\left(A^*\right)\right]A^*A_L}{A_L-A^*}}. \tag{12}$$

From Eq. (10) we have $S_L=\hat{u}^*-u^*=\hat{u}_L-u_L$. We may relate the speed $u^*$ to the parameter $M_L$ and find the following relation for the star velocity:

$$u^*=u_L-f_L\left(A^*,A_L\right)\quad\text{with } f_L\left(A^*,A_L\right)=\sqrt{\frac{\left[gI_1\left(A_L\right)-gI_1\left(A^*\right)\right]\left(A_L-A^*\right)}{A_LA^*}}. \tag{13}$$

The speed $S_L$ can now be calculated, as $A^*$ is known from (9). From (10) we have $S_L=u_L-M_L/A_L$. The velocity of the left shock is then

$$S_L=u_L-\sqrt{\frac{\left[gI_1\left(A_L\right)-gI_1\left(A^*\right)\right]A^*}{\left(A_L-A^*\right)A_L}}. \tag{14}$$

Derivation of the relation for a right shock proceeds in an analogous way to in the case of a left shock. We find the following relations:

$$u^* = u_R + f_R\left(A^*, A_R\right) \quad \text{with } f_R\left(A^*, A_R\right) = \sqrt{\frac{\left[gI_1\left(A_R\right) - gI_1\left(A^*\right)\right]\left(A_R - A^*\right)}{A_R A^*}} \tag{15}$$

$$S_R = u_R + \sqrt{\frac{\left[gI_1\left(A_R\right) - gI_1\left(A^*\right)\right]A^*}{\left(A_R - A^*\right)A_R}}. \tag{16}$$

### 3.3. Rarefaction waves

The case of rarefaction waves is the most difficult as there is no analytical expression of the generalized Riemann invariant (GRI) for the Saint-Venant equations. Indeed, derivation of the GRI [18] leads to the following differential equations that hold across the rarefaction wave:

$$\frac{\mathrm{d}U_1}{r_1^{(L)}} = \frac{\mathrm{d}U_2}{r_2^{(L)}} \Rightarrow \mathrm{d}U + \sqrt{\frac{g}{Al}}\mathrm{d}A = 0 \quad \text{across the left rarefaction} \tag{17}$$

$$\frac{\mathrm{d}U_1}{r_1^{(R)}} = \frac{\mathrm{d}U_2}{r_2^{(R)}} \Rightarrow \mathrm{d}U - \sqrt{\frac{g}{Al}}\mathrm{d}A = 0 \quad \text{across the right rarefaction} \tag{18}$$

where $\mathbf{r}^{(L)}$ and $\mathbf{r}^{(R)}$ are the right eigenvectors of the Jacobian matrix of $\mathbf{F}$ with respect to $\mathbf{U}$ in (5) and correspond to a left and a right rarefaction respectively; and $l$ is the width of the free surface.

Let's consider the relation (17) holding for left rarefaction. We can connect the left state to the star state across the left wave by integrating (17) between $A_L$ and $A^*$ and using the additivity of integration on intervals:

$$\left(U^* - U_L\right) + \underbrace{\int_0^{A^*} \sqrt{g/\alpha l\left(\alpha\right)}\mathrm{d}\alpha}_{\phi^*} - \underbrace{\int_0^{A_L} \sqrt{g/\alpha l\left(\alpha\right)}\mathrm{d}\alpha}_{\phi_L} = 0. \tag{19}$$

Consequently, we have for the left and the right rarefaction

$$u^* = u_L - f_L\left(A^*, A_L\right) \quad \text{with } f_L\left(A^*, A_L\right) = \phi^* - \phi_L \tag{20}$$

$$u^* = u_R + f_R\left(A^*, A_R\right) \quad \text{with } f_R\left(A^*, A_R\right) = \phi^* - \phi_R \tag{21}$$

where the value of the function $\phi$ depends on the geometry of the section.

The speed of the head $S_{HL}$ and the tail $S_{TL}$ of a left rarefaction can also be calculated once $A^*$ is known. It is trivial to show that

$$S_{HL} = u_L - c_L \quad \text{and} \quad S_{TL} = u^* - c^*. \tag{22}$$

To find the solution inside the rarefaction, we consider a point $P = \left(\hat{x}, \hat{t}\right)$ inside the wave and a characteristic joining the origin 0 and $P$. The speed of the characteristic is

$$u - c = \frac{\mathrm{d}x}{\mathrm{d}t} = \frac{\hat{x}}{\hat{t}}. \tag{23}$$

The simultaneous solution of (19) and (23) gives a single non-linear algebraic equation for the flow area $A$ that can be solved iteratively:

$$c(A) + \phi(A) - u_L - \phi_L = 0. \tag{24}$$

The solution for the right rarefaction is found by analogy.

For a rectangular closed pipe, the authors found an analytical formulation for $\phi$:

$$\phi(A) = \int_0^A \sqrt{g/\alpha l\left(\alpha\right)}\mathrm{d}\alpha = \begin{cases} 2\underbrace{\sqrt{gA/l(A)}}_{c(A)} & \text{if } FS \\ 2c(A) + 2\sqrt{gA_{\max}/T_p} - 2\sqrt{gA_{\max}/T_s} & \text{if } PP \end{cases} \tag{25}$$

where $T_p$ is the pipe width, $T_s$ is the Preissmann slot width, and $A_{\max}$ is the cross-sectional area of the pipe (Fig. 3(a)). $A_{\max}$ is the value of $A$ at the pipe crown, the *state FS* indicates that the flow is at a free surface and the *state PP* that the flow is pressurized. If $A > A_{\max}$, the flow is obviously pressurized, *PP*. If $A \leq A_{\max}$, the flow is chosen either pressurized, *PP*, or free

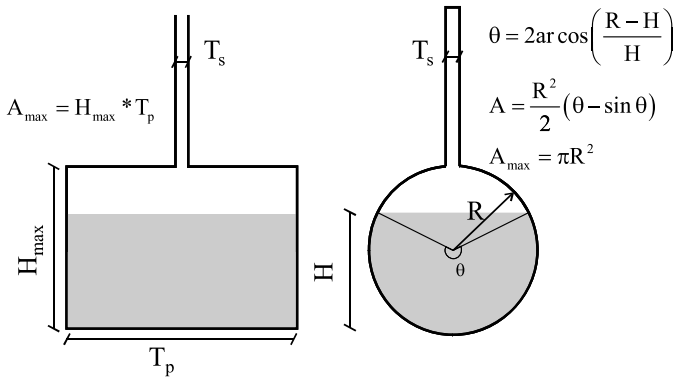


**Fig. 3.** Geometry of the pipe.

surface, *FS*, according to the aeration rate. Lack of aeration devices prevents a free surface from appearing when the pressure drops below the atmospheric pressure. Instead, a sub-atmospheric pressurized flow appears.
Cunge [16] proposes that the formula for the rectangular cross-section should be used in most cases. The authors found that the proposition holds for most prismatic channels. However, a numerical solution may be derived for each geometry. For instance, there is no analytical solution for $\phi$ in the case of a circular pipe of radius $R$ (Fig. 3(b)):

$$\begin{aligned}\phi(A) &= \int_0^A \sqrt{g/\alpha l\,(\alpha)}\mathrm{d}\alpha \\ &= \begin{cases} \sqrt{\dfrac{gR}{4}} \displaystyle\int_0^{\theta} \frac{1-\cos\theta}{\sqrt{\sin\theta/2\,(\theta-\sin\theta)}}\mathrm{d}\theta & \text{if } FS \\ \sqrt{\dfrac{gR}{4}} \displaystyle\int_0^{2\pi} \frac{1-\cos\theta}{\sqrt{\sin\theta/2\,(\theta-\sin\theta)}}\mathrm{d}\theta + 2\sqrt{gA/T_s} - 2\sqrt{gA_{\max}/T_s} & \text{if } PP. \end{cases}\end{aligned} \tag{26}$$

One solution could be to use a numerical integration routine for computing (26). Following Leon [15], we prefer here to use a development in series of the integral (26), which gives good results:

$$\phi(A) = \begin{cases} \sqrt{\dfrac{gR}{4}}\left[\sqrt{3}\theta - \dfrac{\sqrt{3}}{80}\theta^3 + \dfrac{19\sqrt{3}}{448\,000}\theta^5 + \dfrac{\sqrt{3}}{10\,035\,200}\theta^7 + \dfrac{491\sqrt{3}}{27\times 7\,064\,780\,800}\theta^9 + O\left(\theta^{11}\right)\right] & \text{if } FS \\ \phi\,(A_{\max}) + 2\sqrt{gA/T_s} - 2\sqrt{gA_{\max}/T_s} & \text{if } PP. \end{cases} \tag{27}$$

### 3.4. Solution to the Riemann problem

The solution of the Riemann problem is then given by the root of the algebraic equation

$$f\left(A^*\right) \equiv f_L\left(A^*, A_L\right) + f_L\left(A^*, A_R\right) + u_R - u_L = 0 \tag{28}$$

where the functions $f_L$ and $f_R$ are

$$\begin{aligned} f_L\left(A^*, A_L\right) &= \begin{cases} \phi\left(A^*\right) - \phi\left(A_L\right) & \text{if } A^* \le A_L \text{ (rarefaction)} \\ \sqrt{\dfrac{\left[gI_1\left(A_L\right) - gI_1\left(A^*\right)\right]\left(A_L - A^*\right)}{A_L A^*}} & \text{if } A^* > A_L \text{ (shock)} \end{cases} \\ f_R\left(A^*, A_R\right) &= \begin{cases} \phi\left(A^*\right) - \phi\left(A_R\right) & \text{if } A^* \le A_R \text{ (rarefaction)} \\ \sqrt{\dfrac{\left[gI_1\left(A_R\right) - gI_1\left(A^*\right)\right]\left(A_R - A^*\right)}{A_R A^*}} & \text{if } A^* > A_R \text{ (shock)} \end{cases} \end{aligned} \tag{29}$$

with the function $\phi$ given by (25) or (27) or any another relation according to the geometry of the pipe. The solution for the discharge $Q^*$ in the star region follows as

$$Q^* = \frac{A^*}{2}\left(u_R + u_L\right) + \frac{A^*}{2}\left[f_L\left(A^*, A_L\right) + f_L\left(A^*, A_R\right)\right]. \tag{30}$$

The non-linear equation (28) can be solved using a Newton–Raphson iteration procedure:

$$A^*_{k+1} = A^*_k - f\left(A^*_k\right)/f'\left(A^*_k\right) \tag{31}$$

with

$$f'\left(A^*\right) = f'_L\left(A^*\right) + f'_R\left(A^*\right)$$

$$f'_L\left(A^*, A_L\right) = \begin{cases} \phi'\left(A^*\right) & \text{if } A^* \le A_L \text{ (rarefaction)} \\ \dfrac{-c^2\left(A^*\right) A_L A^* \left(A_L - A^*\right) - A_L^2\left(gI_1|_L - gI_1|^*\right)}{2A_L A^* f_L\left(A^*, A_L\right)} & \text{if } A^* > A_L \text{ (shock)} \end{cases} \tag{32}$$

$$f'_R\left(A^*, A_R\right) = \begin{cases} \phi'\left(A^*\right) & \text{if } A^* \le A_R \text{ (rarefaction)} \\ \dfrac{-c^2\left(A^*\right) A_R A^* \left(A_R - A^*\right) - A_R^2\left(gI_1|_R - gI_1|^*\right)}{2A_R A^* f_R\left(A^*, A_R\right)} & \text{if } A^* > A_R \text{ (shock)} \end{cases}$$

where the derivative $\phi'$ is easily computed on the basis of Eqs. (25) and (27).

### 3.5. Sampling the solution

So far we have an algorithm for finding $A^*$ and $Q^*$. However, evaluation of the Godunov flux (7) requires us to compute the solution (28) of the Riemann problem along the axis $x/t = 0$. For this purpose, we apply the same sampling strategy as was introduced in [18]. Speeds of left and right shocks (Eqs. (14) and (16)) and speeds of left and right rarefactions (Eq. (22)) are evaluated. According to the speed values, the solution of the Riemann problem along the axis $x/t = 0$ is $U_L$, $U^*$, $U_R$ or given by (24) if the axis is inside a rarefaction fan. For further details, see [18].

### 3.6. Treatment of the source term

A time-splitting method using a second-order Runge–Kutta discretization is used to introduce source terms into the solution:

$$\begin{aligned} \mathbf{U}_i^{\text{adv}} &= \mathbf{U}_i^n - \frac{\Delta t}{\Delta x}\left[F_{i+1/2} - F_{i-1/2}\right] \\ \mathbf{U}_i^{\text{int}} &= \mathbf{U}_i^{\text{adv}} + \frac{\Delta t}{2}\mathbf{S}\left(\mathbf{U}_i^{\text{adv}}\right) \\ \mathbf{U}_i^{n+1} &= \mathbf{U}_i^{\text{adv}} + \Delta t\mathbf{S}\left(\mathbf{U}_i^{\text{int}}\right). \end{aligned} \tag{33}$$

### 3.7. Boundary conditions

By analogy with [18], we use boundary conditions (BC) of two types. In the presence of solid fixed walls, reflective BC are imposed at the boundaries of the computational domain. In this case, the water section in the "ghost cell" out of the domain is equal to the water section in the adjacent cell. The water velocity in the "ghost cell" is the opposite of the water velocity in the adjacent cell. In the cases in which one is only interested in the local behavior of the solution, one may simulate a transmissive boundary. This type of BC allows waves to pass through. In this case, both the water section and the velocity in the "ghost cell" out of the domain are equal to the water section and velocity in the adjacent cell.

## 4. Model assessment

The model is validated by comparison with analytical, experimental and numerical results for various cases. They involve high velocity transitions, sub-atmospheric pressure, and complex transition configurations.

### 4.1. The Wiggert benchmark

The experimental apparatus used by Wiggert [5] is a horizontal 30 m long, 0.51 m wide flume (Fig. 4). In the middle portion of the flume, a 10 m long roof is installed, creating a closed rectangular pipe 0.51 m in width and 0.148 m in height. The Strickler coefficient is 100 $m^{1/3}/s$ and the pressure wave celerity is 20 m/s (it leads to a slot of 4.62 $10^{-3}$ m width). The initial condition is a stationary state with zero discharge and 0.128 m water level. Then a wave coming from the left side causes a pressurization of the pipe. The water level and pressures in the apparatus are monitored at four locations within the pipe (gauges A to D in Fig. 4). To specify boundary conditions (BC) for the numerical method, Wiggert measured upstream and downstream heads at the tunnel extremities (Fig. 5(a)). In this paper, the time series of the upstream and downstream depths given by Wiggert were digitized and used as BC. Linear interpolation between two adjacent digits is performed. For the velocity, transmissive BC are used.

Fig. 5(b) shows experimental and numerical results for the pressure heads at the four gauges. A rise is observed in the upstream water level of the flume. A transition develops upstream and propagates towards the downstream end of the pipe. An overall satisfactory agreement is observed. In particular, only small numerical oscillations are observed.

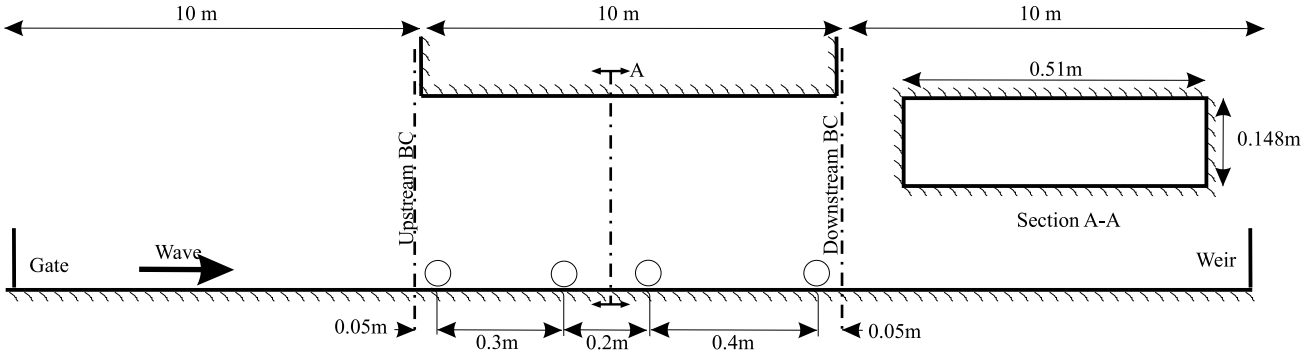


**Fig. 4.** Experimental apparatus of Wiggert.

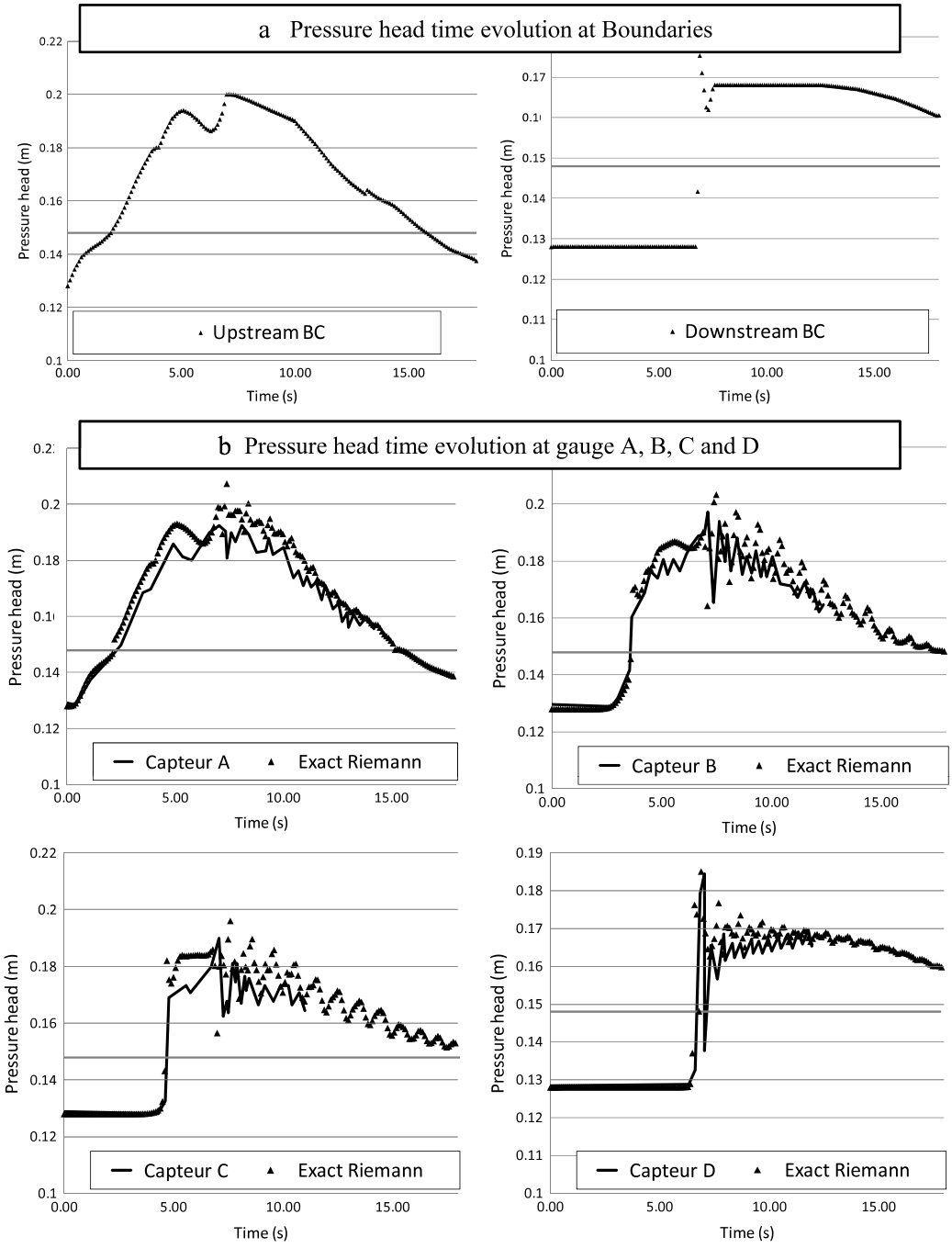


**Fig. 5.** Wiggert benchmark BC and results.

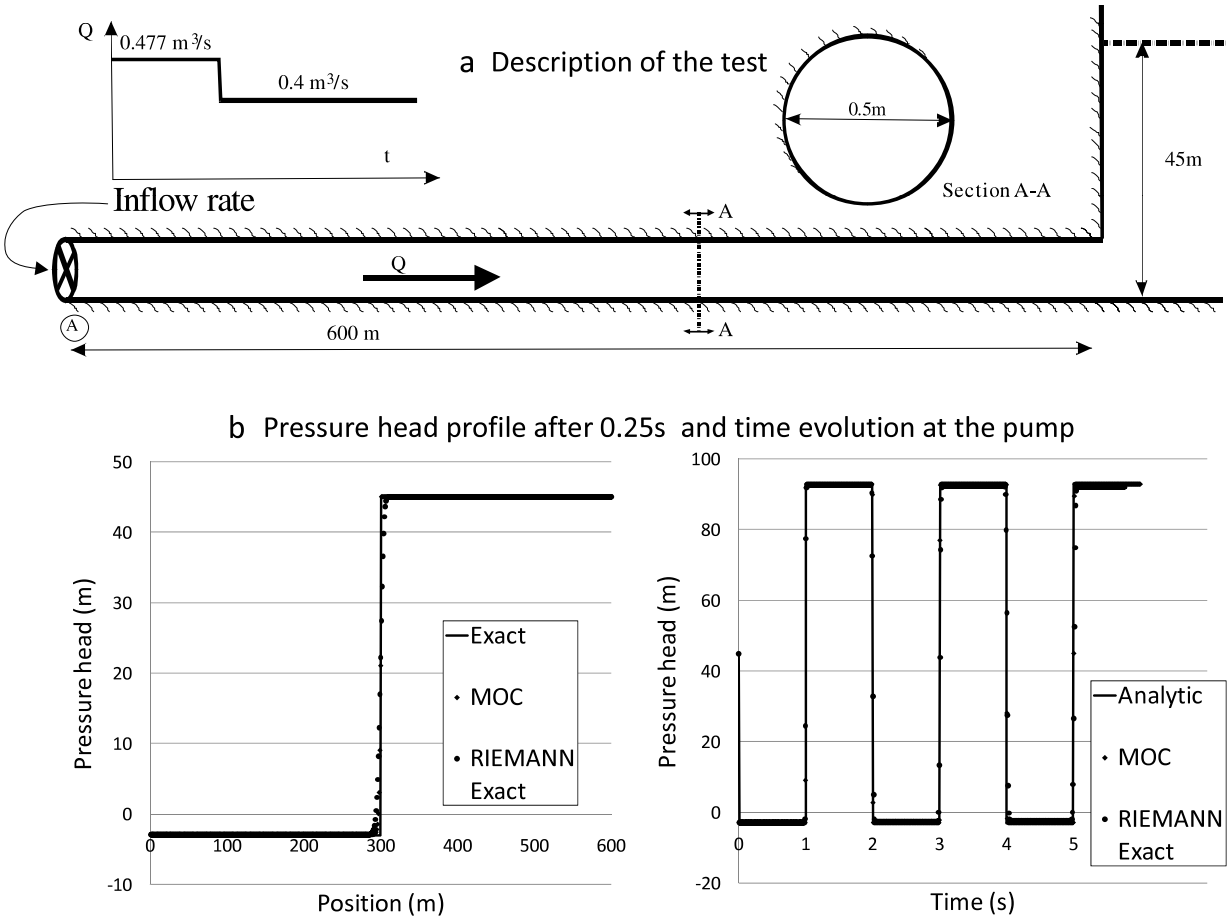


**Fig. 6.** Water hammer test.

### 4.2. A water hammer with sub-atmospheric pressure

The test considers a 600 m long circular pipe of 0.5 m diameter (Fig. 6(a)). The pipe is assumed horizontal and frictionless. The pressure wave celerity is set at 1200 m/s. The initial condition is a steady pressurized state with a discharge of 0.477 $m^3/s$ and a pressure head of 45 m. The downstream pressure head is kept constant at 45 m. At the upstream extremity, the discharge is instantaneously decreased from 0.477 $m^3/s$ down to 0.4 $m^3/s$ in order to produce a highly transient flow. The Joukowsky equation [17] gives an analytical solution for the water hammer pulse induced in such a case:

$$\Delta H = \frac{a\Delta v}{g} = \frac{a\Delta Q}{gA} = \frac{1200 * 0.077}{9.81 * 0.196} = 48.05 \text{ m}. \tag{34}$$

Fig. 6(b) compares the analytical solution of the problem with the results given by the Preissmann slot model with the exact Riemann solver (CFL = 0.96) and by the classical method of characteristics (MOC) scheme [17]. We observe an overall good agreement.

### 4.3. Multiple-point transitions

The analytical benchmark proposed here involves two free-surface/pressurized transitions moving at high velocity. They cross each other, creating a water hammer. The test considers a square pipe of 0.5 m width. It is assumed that the length of the pipe is 50 m, the pressure wave celerity is 50 m/s and the pipe is frictionless. A 0.4 m height of water at rest (no discharge) is chosen as the initial condition. At both extremities of the pipe, the discharge is instantaneously increased from 0.0 $m^3/s$ up to 0.3026 $m^3/s$, resulting in two pressurization bores propagating from extremities up to the center of the pipe. Fig. 7(a) gives a description of the test. An analytical solution is given by the Rankine–Hugoniot relations:

$$\begin{aligned} S_F &= \frac{Q_R - Q_L}{\Omega_R - \Omega_L} \quad \text{(continuity)} \\ S_F &= \frac{Q_R^2/\Omega_R + P_R - Q_L^2/\Omega_L - P_L}{Q_R - Q_L} \quad \text{(momentum)} \end{aligned} \tag{35}$$

where the subscript $.R$ ($.L$) indicates the right (left) side of the bore (Fig. 7(b)). The transition velocity $S_F$ and the post-shock pressure $P_R$ are the two unknowns of the relations. Fig. 8 compares the analytical solution of the problem with the results

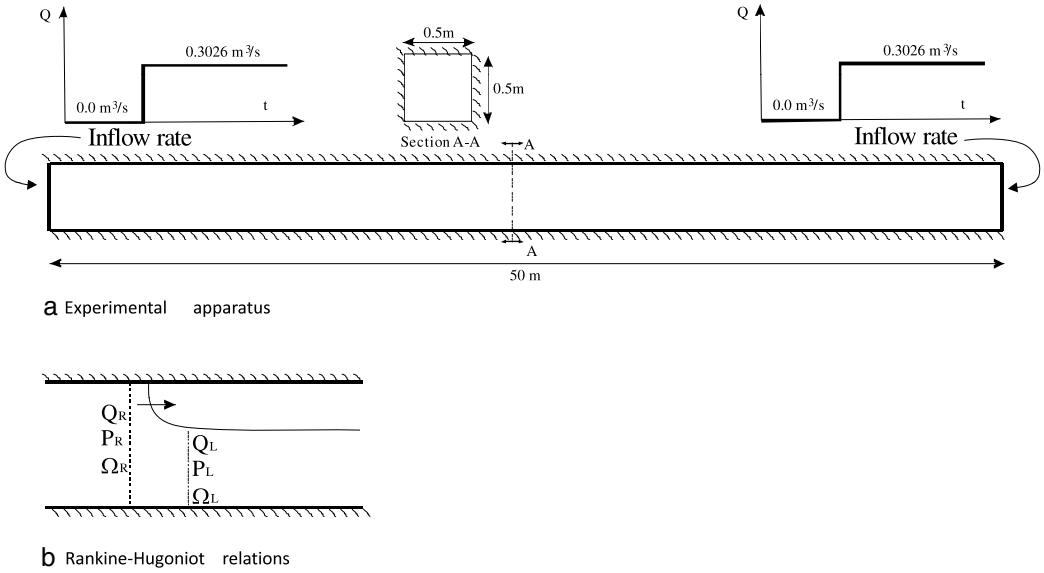


**Fig. 7.** Test of crossing transitions.

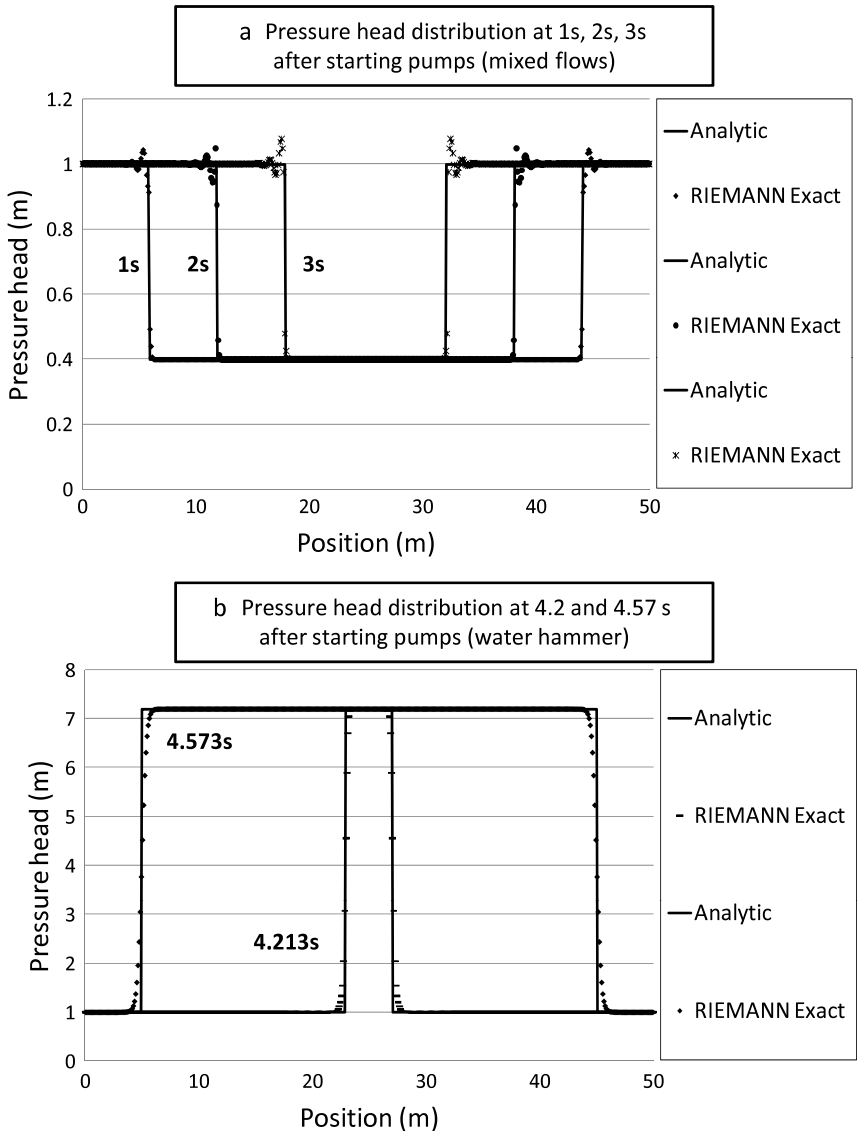


**Fig. 8.** Results of the crossing transitions test.

given by the Preissmann slot model with the exact Riemann solver. The graph represents the pressure head profile at various time steps (Fig. 8). An overall good agreement is observed.

## 5. Conclusions

This work is part of a long term project which aims at developing a hydraulic model for the simulation of highly transient two-phase flow likely to appear in civil and environmental engineering. This requires first an accurate and robust description of free-surface flow and pressurized flow as well as mixed flow. It also entails including air/water interaction in the model. This paper focused mainly on the first issue.

A mathematical model is developed to describe mixed flow on the basis of the Preissmann slot model. A key issue in the equations derived is the ability to simulate sub-atmospheric pressurized flows by means of an original negative Preissmann slot. In addition, a first-order Godunov scheme using an exact Riemann Solver is derived and assessed. The key issue for the Riemann solver is the derivation of a generalized Riemann invariant and a Rankine–Hugoniot relation suitable for the new mathematical model.

The new solver is useful for 1D practical applications involving rectangular and circular pipes. It is also a valuable tool for assessing the performance of other solvers with a wider range of application. Finally, the new solver paves the way to the development of a 2D model for mixed flows and two-phase flow models. Even if the exact Riemann solver dampens their amplitude, post-transition oscillations still appear in the solution for large pressure wave celerities. Obviously, these oscillations are not only linked with the numerical fluxes, so further work is required to find their origin.

## Acknowledgement

This work was supported by the Belgian Fund for Scientific Research F.R.S-FNRS.

## References

[1] Q. Guo, C. Song, Surging in urban storm drainage systems, Journal of Hydraulic Engineering 116 (12) (1990) 1523–1537.
[2] F. Zhou, F.E. Hicks, P.M. Steffler, Transient flow in a rapidly filling horizontal pipe containing trapped air, Journal of Hydraulic Engineering 128 (6) (2002) 625–634.
[3] Q. Guo, C. Song, Dropshaft hydrodynamics under transient conditions, Journal of Hydraulic Engineering 117 (8) (1991) 1042–1055.
[4] J. Vasconcelos, S. Wright, Experimental investigation of surges in a stormwater storage tunnel, Journal of Hydraulic Engineering 131 (10) (2005) 853–861.
[5] D. Wiggert, Transient flow in free-surface, pressurized systems, Journal of the Hydraulics Division, Proceedings of the American Society of Civil Engineers 98 (1) (1972) 11–26.
[6] J. Cardle, C. Song, Mathematical modeling of unsteady flow in storm sewers, International Journal of Engineering Fluid Mechanics 1 (4) (1988) 495–518.
[7] M. Politano, A.J. Odgaard, W. Klecan, Numerical evaluation of hydraulic transients in a combined sewer overflow tunnel system, Journal of Hydraulic Research 133 (10) (2007) 1103–1110.
[8] J. Li, A. McCorquodale, Modeling mixed flow in storm sewers, Journal of Hydraulic Engineering 125 (11) (1999) 1170–1180.
[9] A. Preismann, Propagation des intumescences dans les canaux et rivieres, in: First Congress of the French Association for Computation, Grenoble, France, 1961.
[10] J. Vasconcelos, S. Wright, P.L. Roe, Improved simulation of flow regime transition in sewers: the two-component pressure approach, Journal of Hydraulic Engineering 132 (6) (2006) 553–562.
[11] C. Bourdarias, S. Gerbi, A finite volume scheme for a model coupling free surface and pressurized flows in pipes, Journal of Computational and Applied Mathematics 209 (2007) 109–131.
[12] C. Bourdarias, S. Gerbi, M. Gisclon, A kinetic formulation for a model coupling free surface and pressurized flows in closed pipes, Journal of Computational and Applied Mathematics 218 (2) (2008) 522.
[13] M. Arora, P.L. Roe, On postshock oscillations due to shock capturing schemes in unsteady flows, Journal of Computational Physics 130 (1997) 25–40.
[14] P. Garcia-Navarro, F. Alcrudo, A. Priestley, An implicit method for water flow modelling in channels and pipes, Journal of Hydraulic Research 32 (5) (1994) 721–742.
[15] A. Leon, M. Ghidaoui, A. Schmidt, M. Garcia, Godunov-type solutions for transient flows in sewers, Journal of Hydraulic Engineering 132 (8) (2006) 800–813.
[16] J.A. Cunge, F.M. Holly, A. Verwey, Practical Aspects of Computational River Hydraulics, in: Monographs and Surveys in Water Resources Engineering, vol. 3, Pitman Advanced Pub. Program, Boston, 1980.
[17] E.B. Wylie, V.L. Streeter, Fluid Transients, première ed., M.-H. Inc., 1978, p. 385.
[18] F.E. Toro, Shock-Capturing Methods for Free-Surface Shallow Flows, John Wiley and Sons Ltd., Chichester, NY, Weinheim, Brisbane, Singapore, Toronto, 2000, p. 310.
[19] R.J. Leveque, Finite Volume Methods for Hyperbolic Problems, first ed., in: Cambridge Texts in Applied Mathematics, Cambridge University Press, Cambridge, 2002, p. 540.
[20] P. Glaister, Approximate Riemann solutions of the shallow water equations, Journal of Hydraulic Research 26 (3) (1988) 293–306.